

Experiment and simulation of superconducting magnetic levitation with REBCO coated conductor stacks

Kun Liu¹, Wenjiao Yang¹, Guangtong Ma^{1,3}, Loïc Quéval², Tianyong Gong¹, Changqing Ye¹, Xiang Li¹ and Zhen Luo¹

¹ Applied Superconductivity Laboratory, State Key Laboratory of Traction Power, Southwest Jiaotong University, Chengdu, Sichuan 610031, People's Republic of China

² Group of electrical engineering—Paris (GeePs), CNRS UMR 8507, CentraleSupélec, UPSud, UPMC, Gif-sur-Yvette, France

E-mail: gtma@swjtu.edu.cn

Received 30 July 2017, revised 1 November 2017

Accepted for publication 6 November 2017

Published 4 December 2017



Abstract

Three superconducting stacks made of 120 REBCO coated conductor tapes were each fabricated and assembled to obtain several REBCO modules. Their levitation responses over two different permanent magnet (PM) guideways were investigated by experiment and finite element simulation. For the experiment, a test rig was developed that can measure the force in the three directions for any given relative movement between the REBCO stacks and the PM guideway. For the finite element simulation, a 2D H-formulation was adopted. To treat the high aspect ratio of REBCO tapes, an anisotropic homogenization technique was used. The agreement between the measurements and the simulations is good, thus validating the modeling methodology. It was observed from the experiment and simulation results that the perpendicular field contributes to the levitation force whereas the parallel field is responsible for the guidance force, as a result of the existence of anisotropy on the local magnetic stimulation. Based on that, promising REBCO modules including both longitudinal and transverse arrangements of REBCO stacks were proposed and tested, in terms of providing a significant levitation force with the lateral stability preserved. Moreover, a pre-load process able to suppress the relaxation of the levitation force was put forward. To conclude, this study outlines explicit principles to obtain an appropriate layout of coated conductor stacks that could be effective for practical magnetic levitation operation.

Keywords: coated superconductor tape, magnetic levitation (maglev), finite element methods, levitation force, guidance force

(Some figures may appear in colour only in the online journal)

1. Introduction

Magnetic levitation using high temperature superconducting (HTS) bulk and a permanent magnet (PM) [1] has been substantially advanced in the past decades, and its applications in many industrial fields, such as rail transportation [2–4] and magnetic bearing [5–7], have been demonstrated to be ready for practical deployment. In recent years, an alternative to the HTS bulk was proposed by stacking the REBCO

coated conductor tapes [8]. In comparison with the HTS bulk, the REBCO stack is of much higher critical current density, better thermal stability, larger mechanical strength and more flexible in geometry [9]. Due to these merits and the increasing cost-effectiveness of REBCO coated conductor tapes, the effectiveness of the REBCO stack to act as passive magnetic levitation has been tested by several groups e.g., promising levitation forces have been obtained with stacks of REBCO pancake coils [10], stacks of soldered tapes [11] or stacks of REBCO square annuli [12] by field cooling with a pair of PMs.

³ Author to whom any correspondence should be addressed.

However, the anisotropy of the REBCO stacks, due to the fact that the neighboring layers are electrically isolated, leads to differences between the REBCO stack-type and bulk-type superconducting magnetic levitation that are difficult to explain [11, 13]. Meanwhile, few efforts have been dedicated to improving the guidance force of a REBCO stack despite its importance [14]. Indeed, the levitation and guidance forces are often antagonistic: a relatively low guidance force comes with a high levitation force whereas a relatively low levitation force can come with a high guidance force. This is problematic because the lateral stability is linked to the lateral force. This lack of knowledge leads to a large gap between laboratory-scale superconducting levitation and its practical use. Numerical modeling could help us understand and optimize such systems [15–17]. This is the motivation behind the development and comprehensive validation of the 2D **H**-formulation finite element model presented in this paper.

Additionally, previous studies generally focus on the levitation performances of a single REBCO stack, or of a module made of several stacks having the same arrangement. But the performance of a module made of several stacks having different arrangements has not been reported so far. This will allow us to draw some general conclusions on how to arrange the stacks to achieve a balance between levitation force, guidance force and lateral stability.

This paper is structured as follows. In section 2, we describe in detail the fabrication of the REBCO stacks, the geometry of the PM guideways, as well as the test rig. In section 3, we model the superconducting levitation with the REBCO stacks using a 2D **H**-formulation finite element model. Using these, in section 4, we measure and calculate the levitation performance of a single REBCO stack above two different PM guideways. This reveals how the layout of the REBCO stack affects its levitation performance. In section 5, we investigate the levitation performance of a REBCO module made of three REBCO stacks arranged longitudinally. In section 6, we extend the analysis to a promising REBCO module made of three REBCO stacks arranged transversally. A summary and highlights of the results of this study, together with our outlook, are presented in section 6. A further validation of the numerical model can be found in the [appendix](#).

2. Experimental details

2.1. Fabrication of the REBCO stacks

The HTS REBCO tape used is a 12 mm wide YBCO tape with nonmagnetic substrate from SuperPower Inc. (reference SCS12050-AP). Each stack is made of 120 tapes of 100 mm long, which means that one stack requires 12 m of coated conductor (figure 1(a)).

The stacked REBCO tapes were assembled in a non-magnetic container made of FR4 epoxy resin. In order to impose an appropriate pressure on the REBCO tapes, a convex top cover with stainless steel bolts was designed. This renders the pressure adjustable and the REBCO tapes inside

reusable. The stack has a thickness of 8.5 mm after assembly. The thickness of the bottom and side walls of the container is 2 mm, a tradeoff between magnetic air gap length, mechanical strength and cooling down time. The container with the REBCO tapes is shown in figure 1(b). Three identical containers were made to obtain the REBCO module shown in figure 1(c). The cross-section of each container is sketched in figure 1(d).

To determine the parameters of the REBCO tapes for the simulation, the current-voltage (*I*-*V*) curve of a short sample was measured at 77 K using the four-probe method. The plot is given in figure 2. A power law [18]

$$V = E_c(I/I_{c0})^n l \quad (1)$$

is adopted to fit the measured current-voltage data in order to obtain the tape critical current I_{c0} and the power law index n . With the voltage criterion $E_c = 10^{-4} \text{ V m}^{-1}$, l is the length of short sample which is 15 cm and we have determined $I_{c0} = 387 \text{ A}$ and $n = 31$. This power law will be employed to represent the nonlinear constitutive law of HTS material in the following simulations.

2.2. Geometry of the PM guideways

The two different PM guideways sketched in figure 3 are considered here. The guideway#04 is a pure Halbach array while the guideway#05 uses ferromagnetic pieces to concentrate the field. Both PM guideways are considered for practical applications.

To determine the magnetization M for the simulation, the z -axis component of the magnetic field was measured using a Hall sensor at $z = 6 \text{ mm}$ above the surface of guideway#04 and at $z = 5 \text{ mm}$ above guideway#05. The measured data for both guideways are presented in figure 4. The fitting curves were obtained with a magnetostatic finite element model implemented with the MF physics of Comsol Multiphysics. For the guideway#04, the best fit was obtained with $M = 9.7 \times 10^5 \text{ A} \cdot \text{m}^{-1}$ for all the PMs. For the guideway#05, the best fit was obtained with $M = 8.9 \times 10^5 \text{ A} \cdot \text{m}^{-1}$ for the side PMs and $M = 7.8 \times 10^5 \text{ A} \cdot \text{m}^{-1}$ for the middle PM with a relative magnetic permeability of 4000 for the ferromagnetic pieces.

From figure 4, it is clear that the magnetic field above the center of guideway#04 is dominated by the y -axis component B_y . On the other hand, the magnetic field above the center of guideway#05 is dominated by the z -axis component B_z .

2.3. Layout of the REBCO modules

The three REBCO stacks can be combined in multiple ways to obtain a REBCO module. The layout of the module will have a strong influence on the levitation performance because of the anisotropy of the REBCO tape. The following definitions are adopted to describe the layout. For a longitudinal arrangement (L), the stack is parallel to the x -axis. For a transverse arrangement (T), the stack is parallel to the y -axis. In each arrangement, the surface of the REBCO tape is either parallel (A) or perpendicular (B) to the surface of the PM guideway, i.e., to the

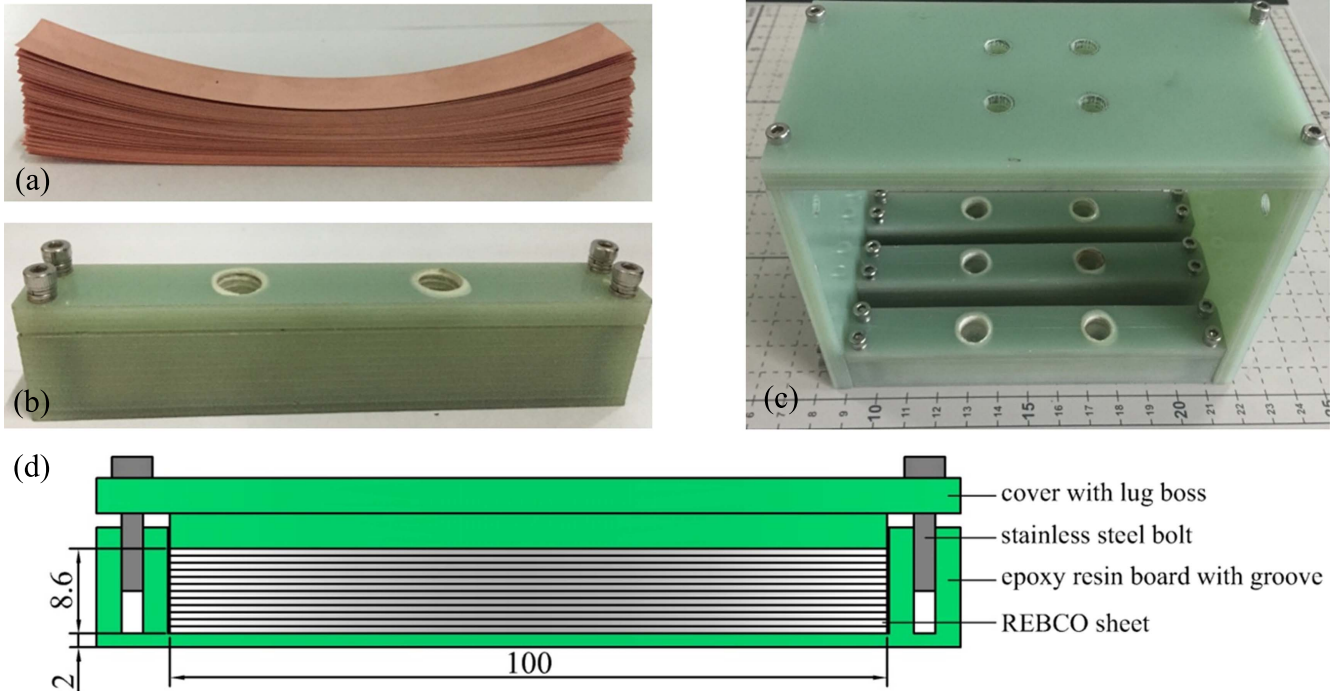


Figure 1. (a) 120 REBCO tapes, (b) REBCO stack inside its container, (c) REBCO module made of three stacks. As shown in the cross-sectional view (d), each REBCO stack has dimensions of 8.5 mm in thickness, 100 mm in length and 12 mm in width (invisible). The container was made of nonmagnetic epoxy resin and has a 2 mm bottom to sustain the attractive force.

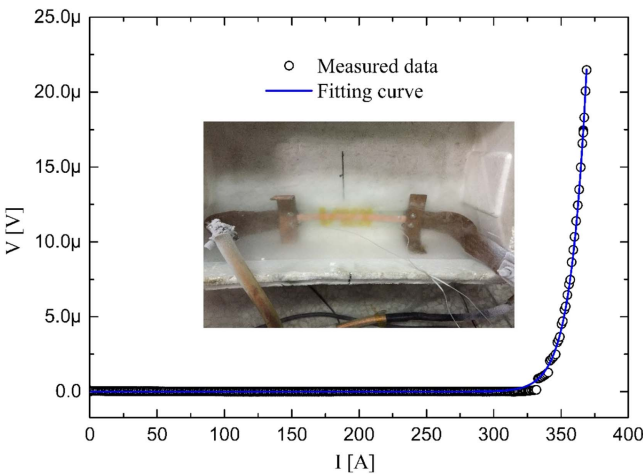


Figure 2. Measured current-voltage relationship of the REBCO tape. The power law (1) was used to fit the measured data. The distance between the two voltage taps was 15 cm.

xy-plane. In this article, we investigate five REBCO modules whose layouts are shown in figure 5 (for the guideway#04). Attempting to maximize the levitation response for both guideways, the distance between two stacks was set to be ~ 25 mm. This option might not be optimal.

2.4. Overview of the test rig

The force measurements were carried out using a test rig developed for this study. Figure 6 shows the test rig while measuring the levitation response of a REBCO module over the guideway#05. The frame of the rig is composed of

standard nonmagnetic aluminum profile and corner fittings. This design makes it lightweight but rigid. The 3D relative motion is executed by three step motors that are connected to the linear guideways via screw rods. The motion is programmed in the processing unit. The 3D position is recorded by three linear displacement sensors. A triaxial tension/compression transducer measures the 3D force up to 500 N, 500 N and 1000 N along the x, y and z-directions, respectively. The time, the 3D position and the 3D force are recorded through a data acquisition and processing unit.

2.5. Test sequences

The coordinate system adopted in this work is shown in figure 3. We consider the two following test sequences:

- *ZFC sequence* (a) The stack/module is cooled down to 77 K at a distance of 100 mm above the center of PM guideway, where the magnetic field of PM guideway can be neglected (zero field cooling). (b) The stack/module is moved vertically downward at 1 mm s^{-1} (quasistatic) until the gap between the stack/module and the PM guideway is 6 mm. (c) The stack/module is moved vertically at 1 mm s^{-1} upward to its initial position. This sequence is used for the calibration of the model.
- *FC sequence* (a) The stack/module is cooled down to 77 K at a distance of 25 mm above the center of PM guideway (field cooling). (b) The stack/module is moved vertically downward at 1 mm s^{-1} (quasistatic) until the gap between the stack/module and the PM guideway is 6 mm. (c) The stack/module is moved vertically at

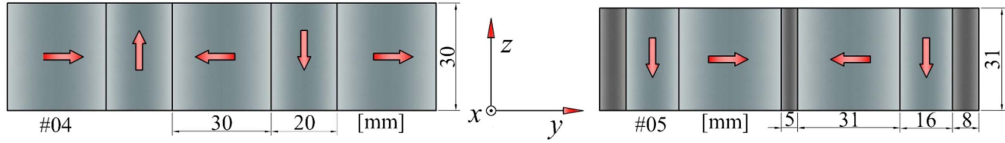


Figure 3. Geometry of the two PM guideways (right). The guideway #04 is a pure Halbach array (left). The guideway #05 uses a ferromagnetic piece as the flux concentrator in its middle and side parts. We have marked these two guideways as #04 and #05 according to the historical identifier of PM guideways fabricated by our laboratory. The arrows indicate the magnetization direction of the PM element in the guideway. In this work, the origin of the Cartesian system is at the center of the upper surface for both guideways.

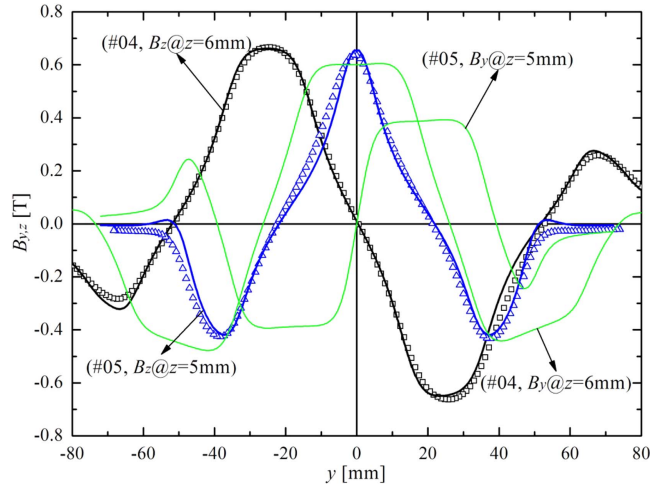


Figure 4. Calculated B_y and B_z distributions (line) of the two PM guideways (#04 and #05). The measured data (symbol) was used to estimate the magnetization of the PM elements in each guideway.

1 mm s⁻¹ upward to its initial position. This sequence is used for the validation of the model.

- **LD sequence** (a) The stack/module is cooled down to 77 K at a distance of 25 mm above the center of the PM guideway. (b) The stack/module is moved vertically downward at 1 mm s⁻¹ until the gap between the stack/module and the PM guideway is 6 mm. (c) The stack/module is moved laterally at 1 mm s⁻¹ with amplitude of 6 mm first to the right, then to the left, and finally back to the center. Such sequence reproduces approximately the regular operation of a magnetic levitation vehicle [19].

3. Numerical model

3.1. H-formulation finite element model

The **H**-formulation with a nonlinear E-J power law is adopted to model the superconductor stacks [20–22]. Starting with Faraday's law $\nabla \times \mathbf{E} + \mu \frac{\partial \mathbf{H}}{\partial t} = 0$ and considering that $\mathbf{J} = \nabla \times \mathbf{H}$, the 2D **H**-formulation reads as

$$\mu \frac{\partial H_y}{\partial t} + \frac{\partial E_x}{\partial z} = 0, \quad (2a)$$

$$\mu \frac{\partial H_z}{\partial t} - \frac{\partial E_x}{\partial y} = 0, \quad (2b)$$

$$J_x = \frac{\partial H_z}{\partial y} - \frac{\partial H_y}{\partial z}, \quad (2c)$$

$$E_x = \rho J_x, \quad (2d)$$

where ρ is the resistivity of the domain.

The PDEs (1a) and (1b) are solved using the 'PDE General Form' in Comsol Multiphysics. The resistivity ρ in the HTS domains is modeled using a nonlinear E-J power law,

$$\rho(J_x) = \frac{E_c}{J_c(\mathbf{B})} \left| \frac{\mathbf{J}}{J_c(\mathbf{B})} \right|^{n-1}, \quad (3)$$

where the field-dependent critical current density $J_c(\mathbf{B})$ is described by an anisotropic Kim-like model [23, 24],

$$J_c(\mathbf{B}) = J_{c0} \left/ \left(1 + \frac{\sqrt{\kappa^2 B_{||}^2 + B_{\perp}^2}}{B_0} \right)^{\alpha} \right., \quad (4)$$

where $B_{||}$ and B_{\perp} are respectively the parallel and perpendicular components of total magnetic flux density (including the self-field effect) with respect to the tape surface. J_{c0} is the self-field critical current density and B_0 , κ and α are material-related parameters.

3.2. Boundary conditions for the superconducting levitation model

To reduce the modeling domain and to avoid the problem of the relative movement, the superconducting levitation model is built by unidirectional coupling between the PM guideway model and the HTS model [15, 16]. The PM guideway model is an **A**-formulation magnetostatic finite element model of the PM guideway alone. The HTS model is an **H**-formulation finite element model of the HTS domain surrounded by a thin air domain (figure 7). The coupling is obtained with Dirichlet boundary conditions applied on the external boundary $\partial\Omega$ of the HTS model [16],

$$H_y(t) = H_y^{\text{ext}}(y(t), z(t)) + H_y^{\text{self}}(t), \quad (5a)$$

$$H_z(t) = H_z^{\text{ext}}(y(t), z(t)) + H_z^{\text{self}}(t), \quad (5b)$$

where H_y^{ext} and H_z^{ext} are respectively the y - and z -component of the external field generated by the PM guideway, and H_y^{self} and H_z^{self} are respectively the y - and z -components of the self-field generated by the supercurrent. The displacement of the REBCO module is modeled by the spatial variation of the external field using the functions $y(t)$ and $z(t)$ which indicate the HTS domain y and z -position. The self-field is calculated

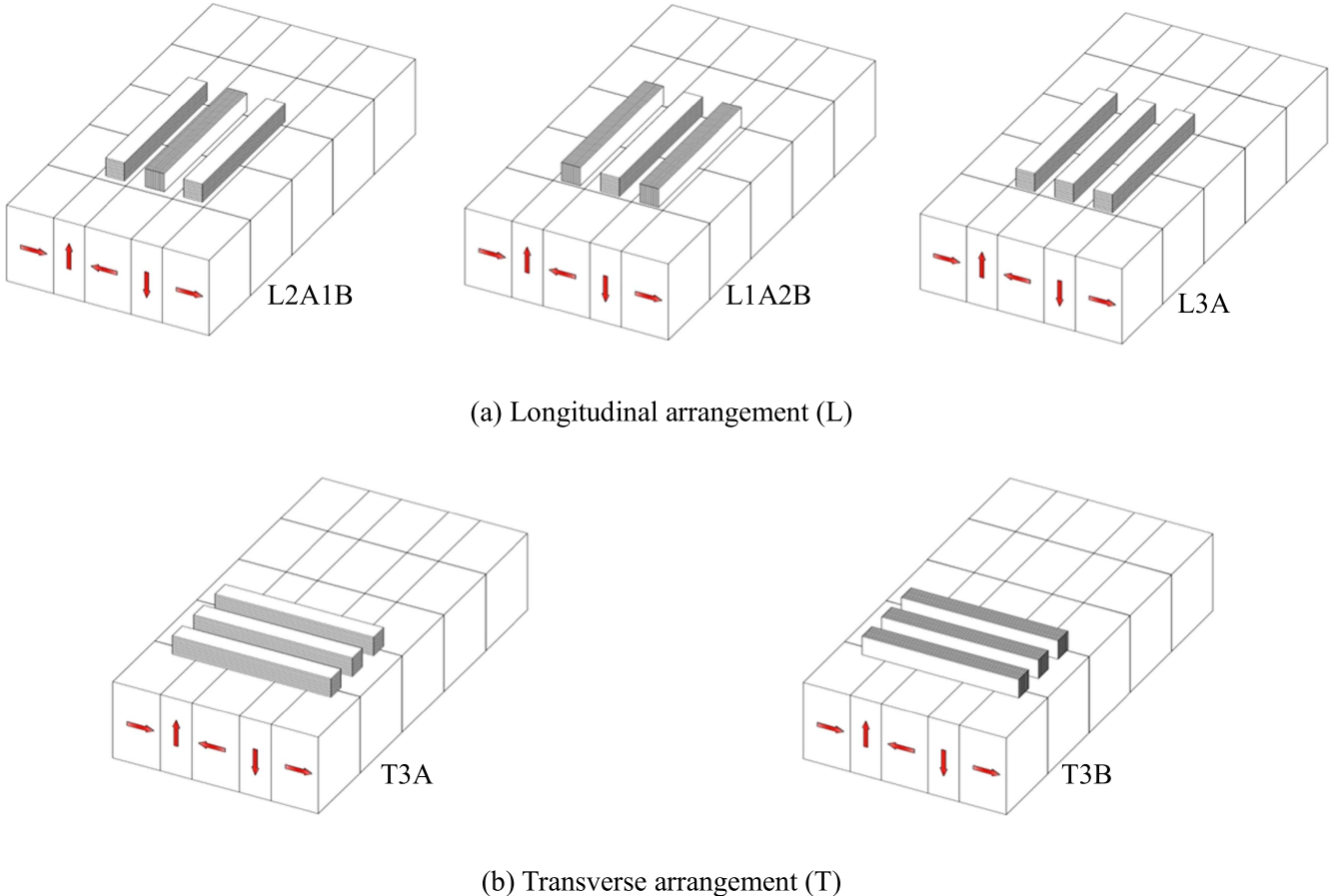


Figure 5. Overview of the five REBCO modules, shown above guideway#04. (a) In the longitudinal arrangement, the stack's length is parallel to the x -direction. (b) In the transverse arrangement, the stack's length is parallel to the y -direction. The tape surface can be either parallel (A) or perpendicular (B) to the upper surface of the PM guideway.

using Biot–Savart's law,

$$H_y^{\text{self}} = -\frac{\mu_0}{2\pi} \iint_s \frac{J_x(z_0 - z)}{(y_0 - y)^2 + (z_0 - z)^2} ds, \quad (6a)$$

$$H_z^{\text{self}} = \frac{\mu_0}{2\pi} \iint_s \frac{J_x(y_0 - y)}{(y_0 - y)^2 + (z_0 - z)^2} ds. \quad (6b)$$

3.3. REBCO stack homogenization

The high aspect ratio of the REBCO tapes can be problematic in the finite element meshing process, leading to a high number of mesh elements and thus to a large computing time [25]. Therefore, similar to what was done in [15], we employ here the anisotropic bulk homogenization technique introduced in [20] and extended in [21] to large stacks and arrays of tapes. Figure 7 illustrates the homogenization process: the REBCO stack is reduced to an anisotropic bulk with equivalent current density $J_{c0,eq}$,

$$J_{c0,eq} = J_{c0} t_{sc} / t_{stack}, \quad (7)$$

where t_{sc} is the total thickness of the superconducting layer, i.e., 120 times the thickness of the superconducting layer of one tape, and t_{stack} is the thickness of the stack. In contrast to

a real REBCO bulk that has a low but non-zero conductivity along its c -axis [26, 27], a stack of a REBCO tape has zero current between the tapes. This anisotropy is described in the numerical model by subdividing the bulk in N_d domains meshed properly [20] and each one having a zero current constraint,

$$\iint_s J_x(t) ds = 0. \quad (8)$$

In practice, the determination of N_d is a compromise between the accuracy and the computing time.

3.4. Model calibration

To calibrate the numerical model, it is common practice to consider the maximum levitation force for the ZFC sequence. Therefore, we measured the levitation force of a single REBCO stack above the center of guideway#05. Using the measured tape critical current density J_{c0} , the permanent magnet magnetization H and the geometric data summarized in table 1, this sequence was simulated with the numerical model described above. The superconductor parameters B_0 , κ and α of (4) were tuned manually so that the hysteresis loop matches the experimental data. Experimental and simulated curves are shown in figure 8. The obtained parameters are

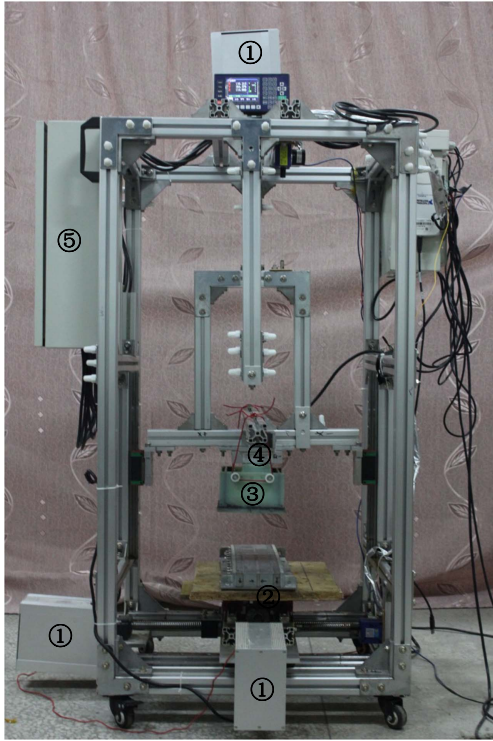


Figure 6. Test rig used to measure the 3D forces of the REBCO stacks/modules over the PM guideways. ① Step motor. ② PM guideway. ③ LN₂ vessel with stacks inside. ④ Triaxial force sensor. ⑤ Data acquisition and processing unit. This test rig is also able to scan the magnetic field above the PM guideway if the force transducer is replaced with a Hall sensor.

summarized in table 1. In the following, the parameters of the numerical model are kept unchanged.

One can see that the simulated curve is able to reproduce correctly the measured F_z in both magnitude and tendency, which is very hard to achieve for superconducting levitation with bulks [16, 17, 28]. This great agreement is mainly due to the fact that (i) the critical current density used in the simulation of REBCO stack was obtained from measurement, not by fitting as needed for bulks and (ii) the 2D simplification is reasonable here as the length in the x -direction is much larger than the characteristic length in the yz -plane.

It is worthy of comment that the accuracy of the simulation could be further improved if a more realistic expression [29–31] could be used to characterize the field and angular dependence of the critical current density in superconductor tapes. In this work, we measured the current-voltage curve of the short tape sample but the complex dataset of the field and orientation dependence of critical current is not available. Due to this limitation, we have to adopt equation (4) to represent the field-dependence of critical current density though more accurate models exist [32–34].

4. REBCO stacks with longitudinal arrangement

The REBCO stack has a high anisotropy and its influence on the levitation performance should be investigated to propose

layouts suitable for practical use. In this regard, we compare in this section four layouts of REBCO stack levitation using a single module. The four layouts named L1A#04, L1B#04, L1A#05 and L1B#05 are shown in figure 9(a). For each one, the levitation and guidance forces for the ZFC, FC and the LD sequences were measured and simulated. The results are plotted in figure 9.

4.1. Levitation force

Figure 9(a) presents the levitation force for the ZFC sequence. Clearly, the magnitude of F_z is highly dependent upon the layout: the largest measured value is over 125 N for L1A#05, whereas the smallest one is nearly zero for L1A#04. For L1A#05, the magnetic field from the guideway#05 is mostly perpendicular to the tape surface, which induces a supercurrent loop within each tape of the stack. In contrast, for L1A#04, the magnetic field from the guideway#04 is mostly parallel to the tape surface, which induces a tape-to-tape current. However, such current cannot survive as the tape-to-tape resistance is high. If one rotates the stack of L1A#04 of 90° around the x -axis, one obtains L1B#04: F_z is greatly improved. This is because for L1B#04, the magnetic field from the guideway#04 is mostly perpendicular to the tape surface, which induces a supercurrent loop within each tape of the stack, similar to L1A#05. Conversely, the magnitude of F_z is considerably reduced if the stack of L1A#05 is rotated by 90° around the x -axis to obtain L1B#05. In this layout, the external field applied to the stack is mostly parallel to the tapes and the induced current is therefore limited by the layer-to-layer resistance. Note that since the y -axis component of magnetic field B_y above the center of guideway#05 is not trivial, the magnitude of F_z for L1B#05 is small but not zero. Figure 9(b) presents the levitation force for the FC sequence. The levitation force exhibits a similar dependence on the layout as for the ZFC case, which implies that the above observations are independent of the cooling condition.

4.2. Guidance force

The inset of figure 9(b) presents the guidance force for the LD sequence for L1A#04 and L1A#05. We observe that the guidance force of L1A#05 has a negative stiffness ($-\partial F_y / \partial y < 0$) leading to lateral instability. Therefore, even if L1A#05 has the highest levitation force capability, it is not suitable for practical magnetic levitation operation which needs both significant levitation and stability. In contrast, the stiffness of F_y for L1A#04 is positive assuring lateral stability. But the levitation force capability of L1A#04 is almost zero making it unattractive. This proves that for REBCO stacks with a longitudinal arrangement, the maximization of the levitation force and the maximization of the guidance force are conflicting objectives.

4.3. Discussion

Overall the simulated curves for both levitation and guidance forces can well reflect the measured data, particularly in the cases involving guideway#05, from which the material-related

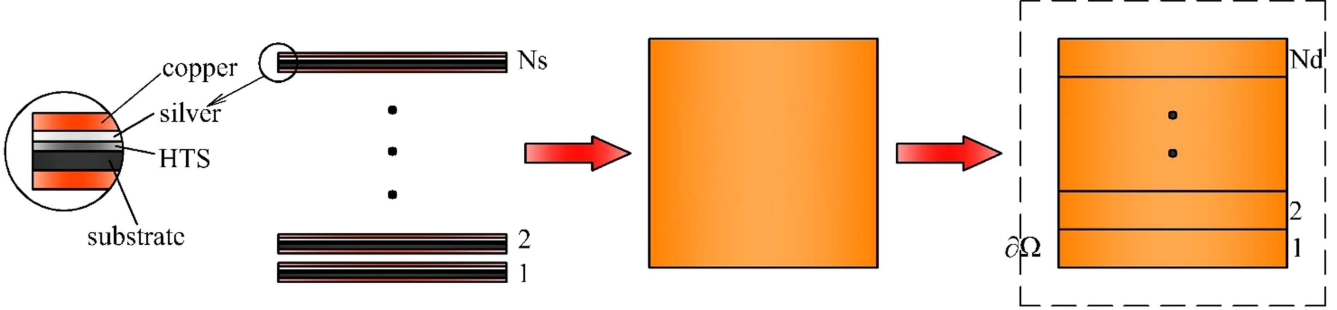


Figure 7. Principle of the homogenization technique applied to treat the high aspect ratio of the REBCO tape. Using this technique, the auxiliary materials of the REBCO tape are neglected and the stack is represented by an anisotropic bulk (there is no inter-tape current).

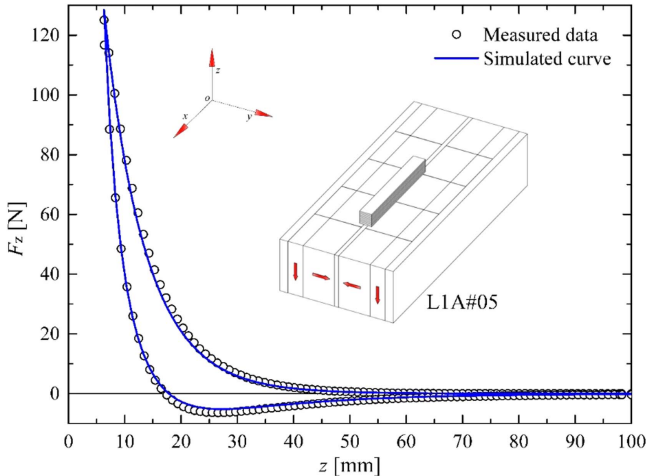


Figure 8. Measured (symbol) and simulated (line) levitation force for the REBCO stack with a longitudinal arrangement above guideway#05 for the ZFC sequence.

parameters of equation (4) were determined. This comprehensive validation confirms the effectiveness of the proposed numerical model to simulate superconducting levitation with a single REBCO stack considering both vertical and lateral movement. Previous stack-type levitation models have been limited to stacks having few tapes [15], neglected the anisotropy of the stack [12], could not include the iron nonlinearity and the exact geometry of the PM guideway [15] or made simplifying assumptions (see the perfectly trapped flux (PTF) model in [10–12] for example).

5. REBCO modules with longitudinal arrangement

We investigate in this section the levitation performance of six layouts of REBCO stack levitation using three modules with longitudinal arrangement. The six layouts named L2A1B#05, L1A2B#05, L3A#05, L2A1B#04, L1A2B#04 and L3A#04 are shown in figures 10(a) and 11(a). For each one, the levitation and guidance forces for the ZFC, FC and the LD sequences were measured and simulated. The results are plotted in figures 10 and 11.

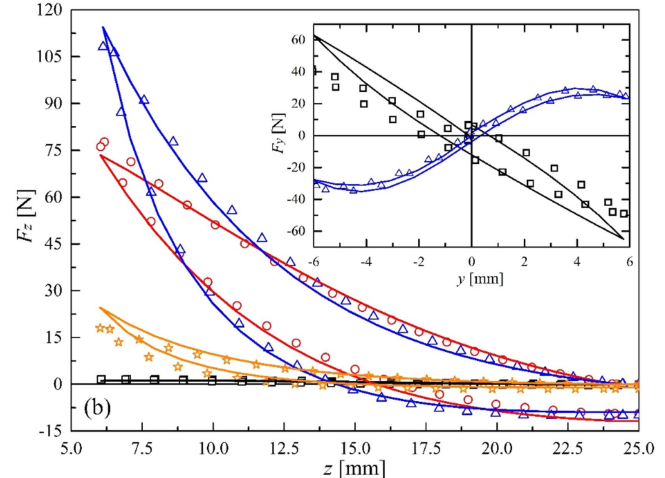
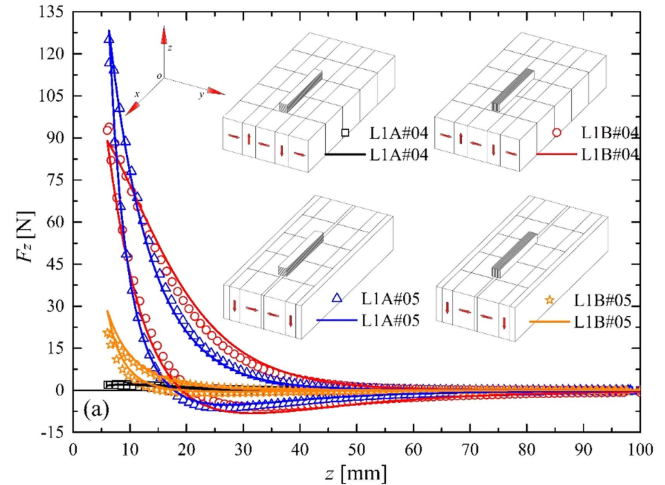


Figure 9. Measured (symbol) and simulated (line) levitation force for the REBCO stacks with a longitudinal arrangement above guideway#04 and guideway#05 (a) for the ZFC sequence and (b) for the FC sequence. Also shown as an inset in (b) is the guidance force for the LD sequence.

5.1. Levitation force

Figure 10(a) presents the levitation force for the ZFC sequence for guideway#05. The highest and lowest F_z were achieved by L1A2B#05 and L2A1B#05, respectively. For L1A2B#05, the magnetic field from the guideway#05 is mostly perpendicular to the tape surface, further implying that

Table 1. Geometrical and material data of the REBCO tapes.

Data of the REBCO tape (Supplier: SuperPower; Type: SCS12050-AP)	
Width [mm]	12
Tape thickness, t_{tape} [μm]	71
Superconducting layer thickness [μm]	1
Critical current (77 K, self-field), I_c [A]	387
Critical current density (77 K, self-field), J_{c0} [$\text{A} \cdot \text{m}^{-2}$]	3.2×10^{10}
Power law index (77 K), n []	31
Criterion of electric field, E_c [$\text{V} \cdot \text{m}^{-1}$]	1×10^{-4}
Material-related parameters in equation (4), B_0 [mT]/ κ/α	$52.5/0.256/0.58$
Data of the REBCO stack	
Width [mm]	12
Thickness, t_{stack} [mm]	8.5
Length [mm]	100
Number of homogenization bulks, N_d	20
Homogenized critical current density, $J_{c0, \text{eq}}$ [$\text{A} \cdot \text{m}^{-2}$]	4.5×10^8

the perpendicular field contributes to the levitation force. For L2A1B#05, the external field is mostly parallel to the tape surface and as the case of the single stack described above, the levitation force is weak due to the difficulty in forming the inter-tape supercurrent. For L3A#05, the middle stack is mainly exposed to fields perpendicular to the tape surface, while the side stacks are exposed to fields parallel to the tape surface. Therefore, only the middle stack provides the levitation force. This explains why F_z is much smaller for L3A#05 than for L1A2B#05, but significantly higher than for L2A1B#05. Figure 10(b) presents the levitation force for the FC sequence for guideway#05. The magnitude of F_z is reduced due to the field cooling process, but the dependence of F_z on the layout remains unchanged.

5.2. Guidance force

The inset of figure 10(b) presents the guidance force for the LD sequence for guideway#05. Although the levitation force of L1A2B#05 is the highest, it is laterally unstable (negative stiffness). Conversely, the levitation force of L2A1B#05 is the lowest, but its guidance force F_y is significant and stable. Therefore, neither layouts L1A2B#05 nor L2A1B#05 are of practical interest for a realistic magnetic levitation system. But L3A#05 is promising as its lateral stability is clear though the magnitude of F_z is relatively low in comparison with L1A2B#05.

Figure 10(c) presents the levitation force for the LD sequence for guideway#05, corresponding to the guidance force F_y in the inset of figure 10(b). During the lateral movement, the value of F_z decreases for each passage at $y = 0$ mm. But the behavior at $y = \pm 6$ mm is complex and depends on the layout: for L1A2B#05 F_z decays; for L2A1B#05 F_z increases; for

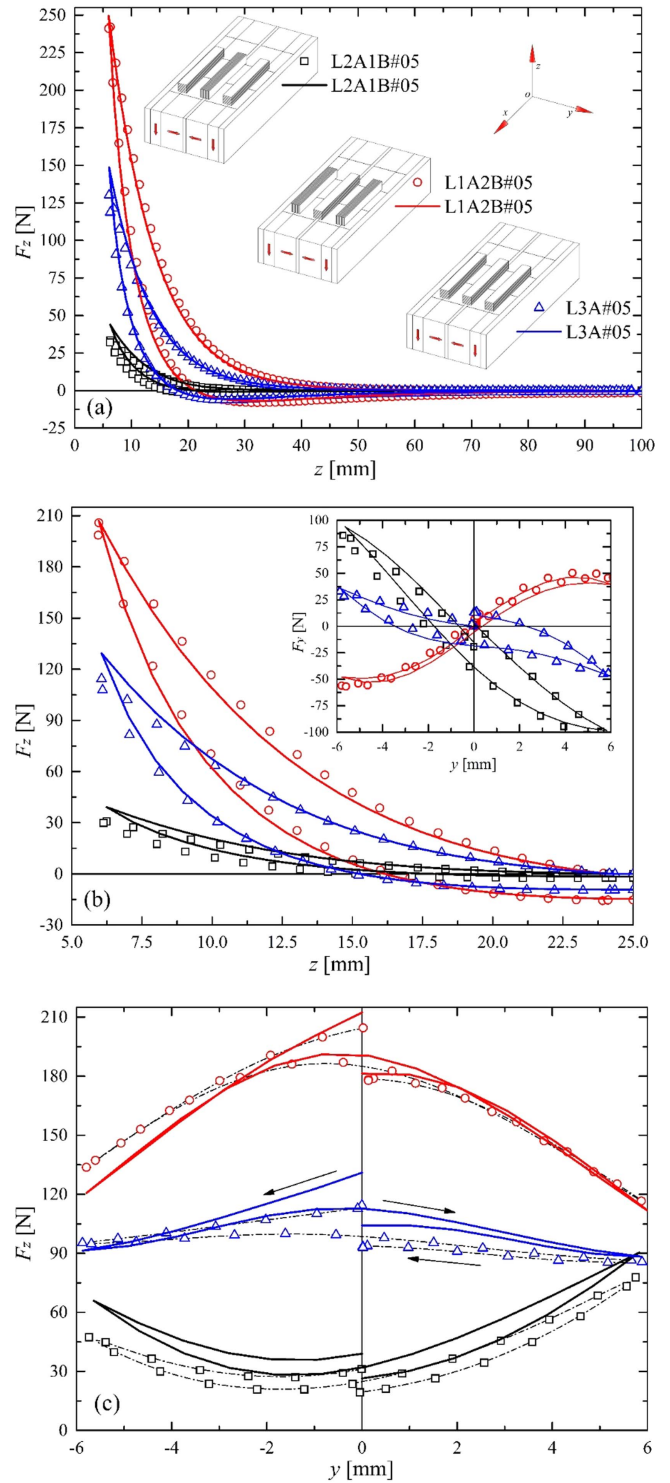


Figure 10. Measured (symbol) and simulated (line) levitation force for the REBCO modules with longitudinal arrangement above guideway#05 (a) for the ZFC sequence condition, (b) for the FC sequence and (c) for the LD sequence (the dashed line is to facilitate the visualization of the sequence). Also shown as an inset in (b) is the guidance force for the LD sequence.

L3A#05 F_z decays but moderately in comparison with L1A2B#05. The behavior of L3A#05 is attributed its ‘midway’ layout between L1A2B#05 and L2A1B#05.

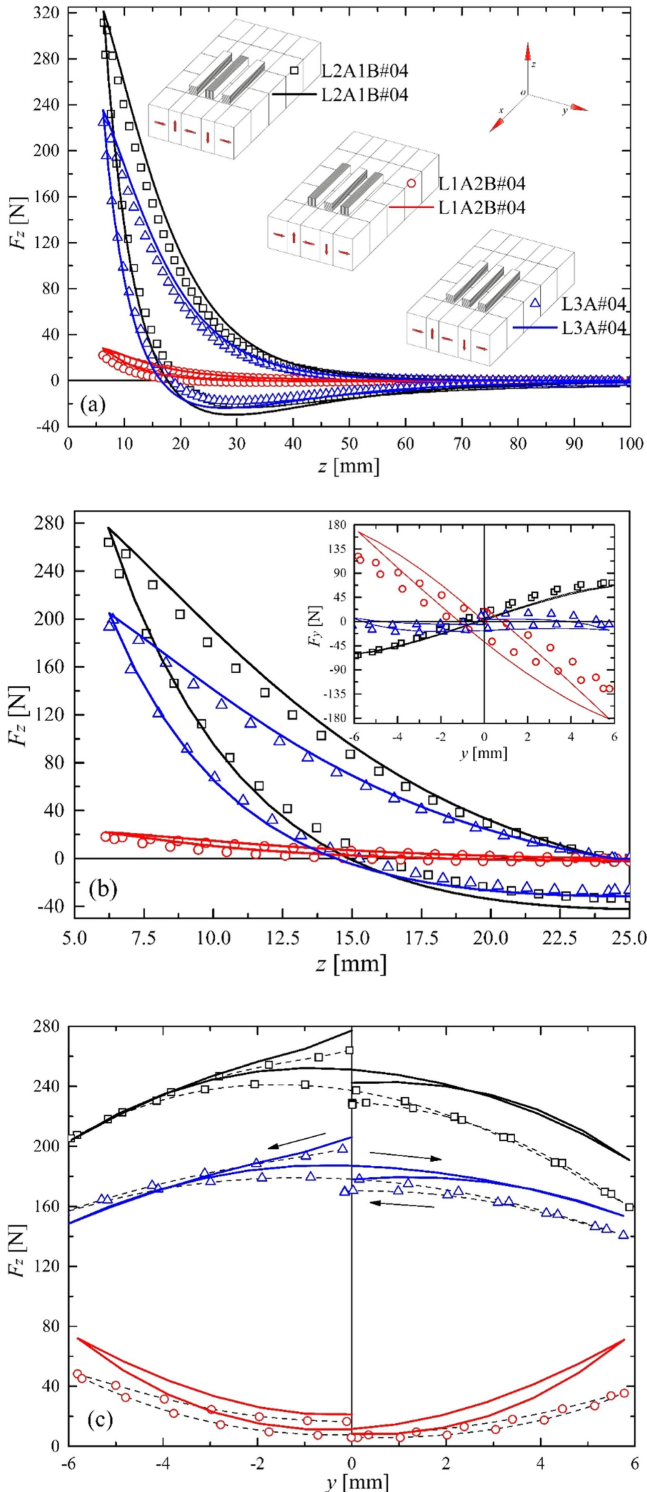


Figure 11. Measured (symbol) and simulated (line) levitation force for the REBCO modules with longitudinal arrangement above guideway#04 (a) for the ZFC sequence condition, (b) for the FC sequence and (c) for the LD sequence (the dashed line is to facilitate the visualization of the sequence). Also shown as an inset in (b) is the guidance force for the LD sequence.

5.3. Discussion

Figure 11 presents results similar to figure 10 but for guideway#04. The above conclusions are confirmed: the PM

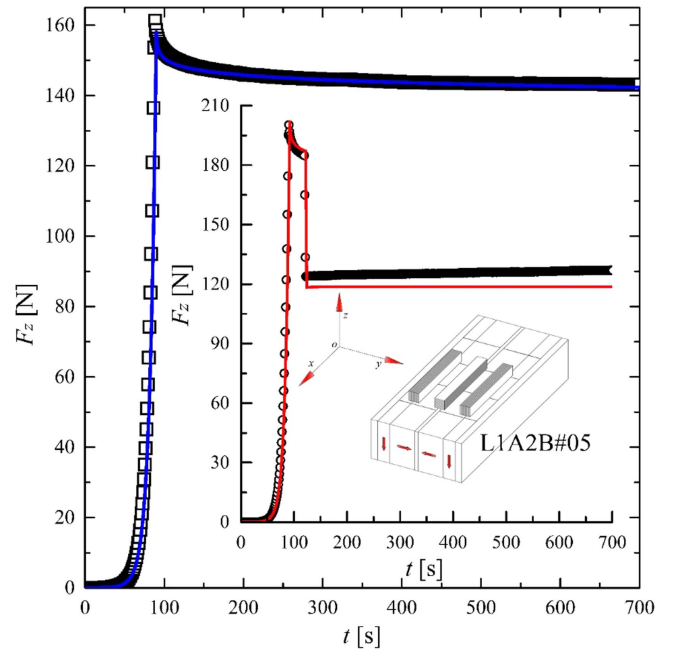


Figure 12. Measured (symbol) and simulated (line) relaxation of the levitation force of the REBCO module with a longitudinal arrangement above guideway#05. Also shown as an inset is the relaxation of the levitation force with pre-load applied.

guideway field being mainly perpendicular to the tape surface, L2A1B#04 presents the highest levitation force but it has a low guidance force. Besides it has negative stiffness, and it is therefore unsuitable for practical use. To the contrary, the PM guideway field being mainly parallel to the tape surface L1A2B#04 has the lowest F_z but the highest guidance force with positive stiffness. The results over guideway#04 demonstrate that the antagonism of the levitation and guidance forces is nearly independent of the PM guideway geometry.

The good agreement between simulations and measurements further confirms the effectiveness of the numerical model. Meanwhile, it confirms the robustness of the numerical model which is able to reproduce the main features of the measurement over the guideway#04, though the fitting parameters were determined from guideway#05.

5.4. Relaxation of the levitation force

The relaxation of the levitation force is crucial as it influences the levitation gap [35]. Thus we measured and calculated the levitation force of L1A2B#05 for a ZFC condition (initial position $z = 100$ m) above the center of the PM guideway, followed by a vertical downward displacement at 1 mm s^{-1} until the gap between the module and the PM guideway was 10 mm. The module is then kept still for 600 s. The results are plotted in figure 12. The levitation force augments quickly with the vertical displacement. Then at a fixed position, the magnitude of F_z decays logarithmically.

The relaxation of the levitation force of the same layout was further studied with a pre-load process [36]. The pre-load process consists of displacing the module from $z = 100$ mm

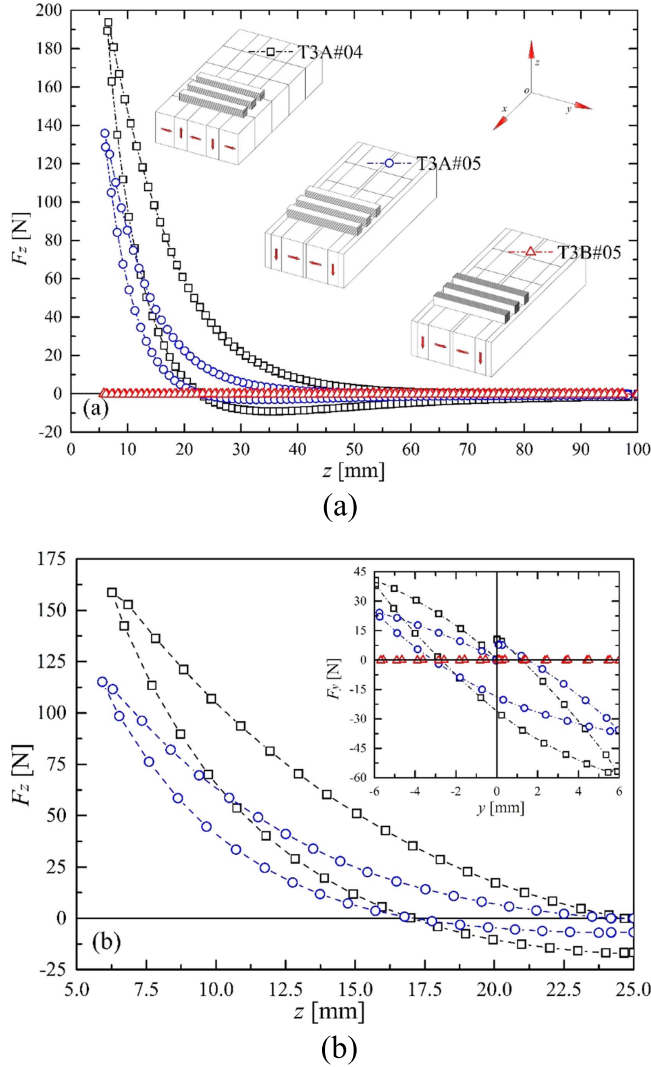


Figure 13. Measured (symbol with dashed line) levitation force of the REBCO module with transverse arrangement above guideway#04 and guideway#05 (a) for the ZFC sequence and (b) for the FC sequence. Also shown as an inset in (b) is the guidance force for the LD sequence.

downwards to $z = 8$ mm and then upwards to $z = 10$ mm. The results are plotted in the insert in figure 12. With pre-load, the decay of the levitation force with time is suppressed, but the magnitude of the force is slightly reduced. This is in accordance with previous experiments with bulk-type levitation [37]. The absence of relaxation decay is favorable as it will not lead to a levitation gap drift which should be avoided in practical use.

Note that the simulated decay of the levitation force agrees quite well with the measurement, except for a slight discrepancy for the pre-load case.

6. REBCO modules with transverse arrangement

We investigate in this section the levitation performance of three layouts of REBCO stack levitation using three modules with transverse arrangement. The three layouts named

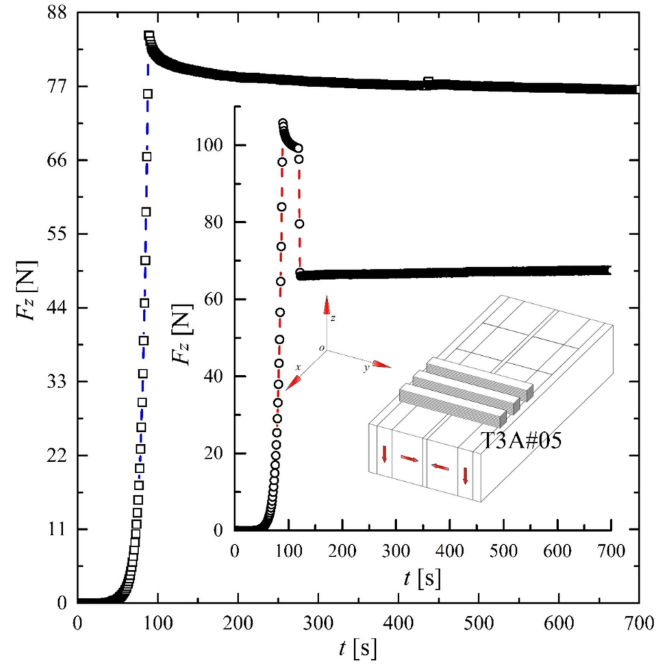


Figure 14. Measured (symbol with dashed line) levitation force relaxation of the REBCO module with transverse arrangement above guideway#05. Also shown as an inset is the relaxation of the levitation force with pre-load applied.

T3A#04, T3A#05 and T3B#05 are shown in figure 13(a). For each one, the levitation and guidance forces for the ZFC, FC and the LD sequences were measured. The results are plotted in figure 13.

6.1. Levitation force

Figure 13(a) presents the levitation force for the ZFC sequence. The T3A#04 layout can provide the largest levitation force but its hysteresis loop is also the widest. This is because the cross-section of the guideway#04 is larger than that of guideway#05 (3900 mm^2 vs. 3565 mm^2), and because it concentrates more of the magnetic field. But the T3B#05 layout provides no levitation force for both guideways. This is because the field generated by the PM guideways is always parallel to the tape surface. Figure 13(b) presents the levitation force for the FC sequence. The observed tendency is the same as for the ZFC case, though the magnitude of F_z is reduced.

6.2. Guidance force

The inset of figure 13(b) presents the guidance force for the LD sequence. For the both PM guideways, the T3A layout proves to be stable against the lateral movement (positive stiffness), while the T3B layout shows no guidance force for the same reason as stated above. This suggests that the T3A layout is a promising candidate for magnetic levitation applications because it can provide both significant levitation and stable guidance force.

6.3. Relaxation of the levitation force

Furthermore, the relaxation of the levitation force with and without pre-load was measured for the T3A#05 layout. The results are shown in figure 14. The measurement conditions were the same as those in figure 12, with similar conclusions: logarithmic decay of the levitation force without pre-load and no decay with pre-load.

6.4. Discussion

For the REBCO modules with transverse arrangement, the 2D numerical model is not adapted because the dimension of each stack along the x -axis is only 12 mm. A 3D model would be necessary in this case for further study.

7. Summary and outlook

Through experimental and numerical means, we investigated the levitation performance of various layouts of REBCO stack levitation with REBCO modules, we come to the conclusions that:

- (i) Because of the anisotropy of REBCO stacks, their levitation performance is highly dependent on the magnetic field stimulation. A magnetic field perpendicular to the tape surface contributes to the force thanks to the supercurrent induced in each tape of the stack. But a magnetic field parallel to the tape surface produces no force. This is due to the low tape-to-tape conductivity preventing any strong induced current. This allows us to understand the measured levitation performance of various REBCO modules.
- (ii) The REBCO module with longitudinal arrangement having all the tapes placed perpendicular to the local PM guideway field can provide the highest levitation force. But for a lateral movement, the local field will become parallel to the tapes and the guidance force will be low with negative stiffness. Conversely, the levitation force is low but the guidance force is high if all the tapes are parallel to the local magnetic field. Therefore an intermediate layout has the potential of providing a significant levitation force with sufficient guidance force and positive stiffness, if properly designed.
- (iii) The REBCO module with transverse arrangement having the tapes placed parallel to the PM guideway surface is promising for realistic applications that require a significant levitation force, as well as a guidance force with positive stiffness. To the contrary, the transverse arrangement having the tapes placed perpendicular to the PM guideway surface has neither a levitation force nor guidance force as the PM guideway field is parallel to the tape surface.
- (iv) A logarithmic relaxation of the levitation force has been observed for stack-type levitation, similar to bulk-type levitation. It was demonstrated that this decay can be suppressed by a pre-load process consisting of bringing

the module to a height smaller than the working height. This study confirms the effectiveness of the pre-load process to enhance the levitation performance of both stack- and bulk-type levitation.

- (v) The proposed 2D \mathbf{H} -formulation finite element model can predict accurately the performance of the REBCO stack-type levitation. For calibration, it requires the knowledge of the magnetization M of the magnets, the critical current density J_{c0} of the REBCO tapes and the power law index n , that can all be obtained from distinct measurements. Note that such a good agreement is difficult to obtain with bulk-type levitation for which the critical current density is a tuning parameter.

The REBCO tapes commercially available are mostly developed for power systems and high field magnets, where the primary concerns are the joint-free length and the uniformity of the critical current. In this context, the width of REBCO tapes is often less than 12 mm. However, for REBCO stack-type levitation, the requirements for the material are quite different. As a stack can be made of several hundreds of short length tapes, the production joint-free length is not a concern. Moreover, the critical current is still a key target but its uniformity is not critical because a defect would only affect the local tape. But for magnetic levitation use, tapes having a large width are desirable in order to increase the size of the supercurrent loop and enhance the levitation capability [38]. The fabrication of REBCO tapes with large width is technically realizable. AMSC already produces 46 mm wide tapes [12] but it uses a ferromagnetic substrate whose effects on the levitation performance have not yet been clarified. Meanwhile, the auxiliary layers in the REBCO tape should be as thin as possible in order to increase the engineering current density. This is feasible as the quench of the REBCO tape used for levitation use is not an issue, allowing the thickness of the constituents to protect the superconducting layer during a quench to be minimized. Fortunately, technical advances towards this direction have been recently achieved, i.e., the substrate has been decreased to 30 μm thick while improving the engineering critical current [39]. In addition, from an economic point of view, one can use REBCO tapes that would not be suitable for power systems applications to construct REBCO stacks for levitation, thus reducing the demands on the length. This emerging stack-type levitation, with more effort to adapt the conductor for such use, will become a competitive alternative to the traditional bulk-type levitation, whose capability seems to reach a plateau.

Acknowledgments

The authors would like very much to thank the anonymous reviewers, whose critical comments considerably improved the quality of this paper. This work was supported in part by the National Natural Science Foundation of China under Grants 51475389, 51722706 and 51707164, in part by the Sichuan Youth Science&Technology Foundation under Grant

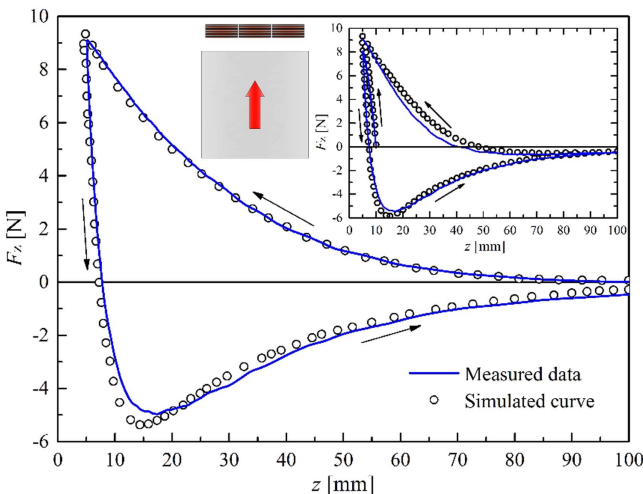


Figure A1. Validation of the numerical model by comparison with the measured levitation force of three REBCO stacks over a square PM for a zero field cooling sequence and (inset) a field cooling sequence (sequences different from the ones used in this article).

2016JQ0003, in part by the Fundamental Research Funds for the Central Universities under Grant 2682016ZY05, in part by the State Key Laboratory of Traction Power under Grants TPL1712 and 2015TPL_T05.

Appendix. Validation of the numerical model by other measured data

The numerical model developed in section 3 is further validated using data measured by another group [15]. There, the PM is a NdFeB magnet with dimensions of 100 mm \times 50 mm \times 50 mm, respectively in the x -, y -, and z -directions. The coercive force of the magnet is 780 kA·m $^{-1}$. Each REBCO stack contains ten pieces of 12 mm wide HTS tape from SuperPower Inc., and has a length of 67 mm in the x -direction. The HTS tapes we employed in this work are the same type, and therefore for this simulation we can use the material parameters summarized in table 1.

Both the ZFC and FC conditions were simulated and compared with the experimental data. For the ZFC condition, the REBCO stack is cooled down at $z = 100$ mm above the PM surface. Then it is moved vertically downwards to $z = 5$ mm. Then it is moved back to its initial position. For the FC condition, the REBCO stack is cooled down at $z = 10$ mm above the PM surface. Then it is moved vertically downwards to $z = 5$ mm, and upwards until $z = 100$ mm and finally back to its initial position. The speed was set at 0.5 mm·s $^{-1}$. The results are shown in figure A1. The simulated levitation forces are in good agreement with the forces measured in both conditions, though a small discrepancy between them exists in the ascending branch of the ZFC case or in the descending branch of the FC case from $z = 100$ mm. This further validates the numerical model.

ORCID iDs

Guangtong Ma <https://orcid.org/0000-0002-0249-4310>

References

- [1] Brandt E 1989 Levitation in physics *Science* **243** 349
- [2] Wang J S *et al* 2002 The first man-loading high temperature superconducting Maglev test vehicle in the world *Physica C* **378–381** 809–14
- [3] Schultz L, Haas O D, Verges P, Beyer C, Röhlig S, Olsen H, Kühn L, Berger D, Noteboom U and Funk U 2005 Superconductively levitated transport system—The SupraTrans project *IEEE Trans. Appl. Supercond.* **15** 2301
- [4] Sotelo G G, de Oliveira R A H, Costa F S, Dias D H N, de Andrade R Jr and Stephan R M 2015 A full scale superconducting magnetic levitation (maglev) vehicle operational line *IEEE Trans. Appl. Supercond.* **25** 3601005
- [5] Werfel F N, Floegel-Delor U, Rothfeld R, Riedel T, Goebel B, Wippich D and Schirrmüller P 2012 Superconductor bearings, flywheels and transportation *Supercond. Sci. Technol.* **25** 014007
- [6] Ogata M, Matsue H, Yamashita T, Hasegawa H, Nagashima K, Maeda T, Matsuoka T, Mukoyama S, Shimizu H and Horiuchi S 2016 Test equipment for a flywheel energy storage system using a magnetic bearing composed of superconducting coils and superconducting bulks *Supercond. Sci. Technol.* **29** 054002
- [7] Mukoyama S *et al* 2017 Development of superconducting magnetic bearing for 300 kW flywheel energy storage system *IEEE Trans. Appl. Supercond.* **27** 3600804
- [8] Sass F, Sotelo G G, Polasek A and de Andrade R 2011 Application of 2G-tape for passive and controlled superconducting levitation *IEEE Trans. Appl. Supercond.* **21** 1511
- [9] Samoilov S, Molodyk A, Lee S, Petrykin V, Valitka V, Martynova I, Makarevich A, Markelov A, Moyzykh M and Blednov A 2016 Customised 2G HTS wire for applications *Supercond. Sci. Technol.* **29** 024001
- [10] Patel A, Hopkins S C, Baskys A, Kalitka V, Molodyk A and Glowacki B A 2015 Magnetic levitation using high temperature superconducting pancake coils as composite bulk cylinders *Supercond. Sci. Technol.* **28** 115007
- [11] Patel A, Kalitka V, Hopkins S C, Baskys A, Figin Albisetti A, Giunchi G, Molodyk A and Glowacki B A 2016 Magnetic levitation between a slab of soldered HTS tape and a cylindrical permanent magnet *IEEE Trans. Appl. Supercond.* **26** 3601305
- [12] Patel A, Hahn S, Voccio J, Baskys A, Hopkins S C and Glowacki B A 2017 Magnetic levitation using a stack of high temperature superconducting tape annuli *Supercond. Sci. Technol.* **30** 2017
- [13] Sass F, Dias D H N, Sotelo G G and de Andrade R 2013 Superconducting levitation using coated conductors *IEEE Trans. Appl. Supercond.* **23** 3600905
- [14] Sass F, Dias D H N, Sotelo G G and de Andrade R 2014 Lateral displacement influence on the levitation force of YBCO coated conductor linear bearings *IEEE Trans. Appl. Supercond.* **24** 3600405
- [15] Sass F, Sotelo G G, de Andrade R and Sirois F 2015 H-formulation for simulating levitation forces acting on HTS bulks and stacks of 2G coated conductors *Supercond. Sci. Technol.* **28** 125012
- [16] Quéval L, Sotelo G G, Kharmiz Y, Dias D H N, Sass F, Zermeño V M R and Gottkehaskamp R 2016 Optimization

- of the superconducting linear magnetic bearing of a maglev vehicle *IEEE Trans. Appl. Supercond.* **26** 3601905
- [17] Ye C Q, Ma G T and Wang J S 2016 Calculation and optimization of high-temperature superconducting levitation by a vector potential method *IEEE Trans. Appl. Supercond.* **26** 360330
- [18] Grilli F, Stavrev S, Le Floch Y, Costa-Bouzo M, Vinot E, Klutsch I, Meunier G, Tixador P and Dutoit B 2005 Finite-element method modeling of superconductors: from 2D to 3D *IEEE Trans. Appl. Supercond.* **15** 1
- [19] Sotelo G G, de Andrade R, Dias D H N, Ferreira A C, Costa F, Machado O J, de Oliveira R A H, Santos M D A and Stephan R M 2013 Tests with one module of the Brazilian Maglev-Cobra vehicle *IEEE Trans. Appl. Supercond.* **23** 3601204
- [20] Brambilla R, Grilli F and Martini L 2007 Development of an edge-element model for ac loss computation of high-temperature superconductors *Supercond. Sci. Technol.* **20** 16–24
- [21] Zermeño V M R, Abrahamsen A B, Mijatovic N, Jensen B B and Sørensen M P 2013 Calculation of alternating current losses in stacks and coils made of second generation high temperature superconducting tapes for large scale applications *J. Appl. Phys.* **114** 173901
- [22] Quéval L, Zermeño V M R and Grilli F 2016 Numerical models for AC loss calculation in large-scale applications of HTS coated conductors *Supercond. Sci. Technol.* **29** 2
- [23] Kim Y B, Hempstead C F and Strnad A R 1962 Critical persistent currents in hard superconductors *Phys. Rev. Lett.* **9** 306
- [24] Gömöry F, Vojenčiak M, Pardo E, Solovyov M and Šouc J 2010 AC losses in coated conductors *Supercond. Sci. Technol.* **23** 034012
- [25] Zermeño V M R, Mijatovic N, Traeholt C, Zirngibl T, Seiler E, Abrahamsen A B, Pedersen N F and Sørensen M P 2011 Towards faster FEM simulation of thin film superconductors: a multiscale approach *IEEE Trans. Appl. Supercond.* **21** 3273–6
- [26] Ma G T, Wang J S and Wang S Y 2010 3D modeling of high-T_c superconductor for magnetic levitation/suspension application—Part I: introduction to the method *IEEE Trans. Appl. Supercond.* **20** 2219
- [27] Ma G T, Wang J S and Wang S Y 2010 3D modeling of high-T_c superconductor for magnetic levitation/suspension application—Part II: validation with experiment *IEEE Trans. Appl. Supercond.* **20** 2228
- [28] Ye C Q, Ma G T and Wang J S 2016 Calculation and optimization of high-temperature superconducting levitation by a vector potential method *IEEE Trans. Appl. Supercond.* **26** 3603309
- [29] Pardo E and Grilli F 2012 Numerical simulations of the angular dependence of magnetization AC losses: coated conductors, Roebel cables and double pancake coils *Supercond. Sci. Technol.* **25** 014008
- [31] Gömöry F, Šouc J, Pardo E, Eugen Seiler E, Solovyov M, Frolek L, Skarba M, Konopka P, Pekarčíková M and Janovec J 2013 AC loss in pancake coil made from 12 mm wide REBCO tape *IEEE Trans. Appl. Supercond.* **23** 5900406
- [32] Grilli F, Sirois F, Zermeño V M R and Vojenčiak M 2014 Self-consistent modeling of the *I_c* of HTS devices: how accurate do models really need to be? *IEEE Trans. Appl. Supercond.* **24** 8000508
- [33] Hu D, Ainslie M D, Raine M J, Hampshire D P and Zou J 2016 Modeling and Comparison of In-Field Critical Current Density Anisotropy in High-Temperature Superconducting (HTS) Coated Conductors *IEEE Trans. Appl. Supercond.* **26** 6600906
- [34] Zermeño V M R, Habelok K, Stepień M and Grilli F 2017 A parameter-free method to extract the superconductor's *J_c(B, θ)* field-dependence from in-field current–voltage characteristics of high temperature superconductor tapes *Supercond. Sci. Technol.* **30** 031001
- [35] Abin D, Osipov M, Pokrovskii S and Rudnev I 2016 Relaxation of levitation force of a stack of HTS tapes *IEEE Trans. Appl. Supercond.* **26** 8800504
- [36] Ma G T, Lin Q X, Wang J S, Wang S Y, Deng Z G, Lu Y Y, Liu M X and Zheng J 2008 Method to reduce levitation force decay of the bulk HTSC above the NdFeB guideway due to lateral movement *Supercond. Sci. Technol.* **21** 065020
- [37] Wang J C, Jiang G Q, Xu Y Y, Wang N, Ma G T, Liu W, Jiang D H and Lin Q X 2011 Relaxation characteristic of the levitation force of bulk Y-Ba-Cu-O with pre-loading applied *Cryo. Supercond.* **39** 7 (in Chinese)
- [38] Ma G T, Ye C Q, Liu K, Mei G M, Zhang H and Li X T 2016 Geometrical effects on the levitation capability of multiseeded Y-Ba-Cu-O blocks *IEEE Trans. Appl. Supercond.* **26** 3600205
- [39] Sundaram A et al 2016 2G HTS wires made on 30 μm thick Hastelloy substrate *Supercond. Sci. Technol.* **29** 104007